

# Flame Retarding Polyamide 11 with exfoliated vermiculite nanoflakes

Afonso D. Macheça<sup>a,#</sup>, Walter W. Focke<sup>a,\*</sup>, Mustapha Kaci<sup>a,b</sup>, Bindu Panampilly<sup>a</sup> and René Androsch<sup>c</sup>

<sup>a</sup>Institute of Applied Materials, Department of Chemical Engineering, University of Pretoria, Private Bag X20, Hatfield 0028, South Africa

<sup>b</sup>Laboratoire des Matériaux Polymères Avancés (LMPA), Faculté de Technologie, Université de Bejaia 06000, Algeria

<sup>c</sup>Interdisciplinary Center for Transfer-oriented Research in Natural Sciences (IWE TFN), Martin Luther University Halle-Wittenberg, 06099 Halle/Saale, Germany

## Abstract

Polyamide 11-based bionanocomposites were prepared by melt compounding with 10 wt.% clays of different chemistry and morphology. This included vermiculite nanoflakes obtained by consecutive thermal and ultrasonic exfoliation in both neat and organo-modified form. The mechanical reinforcement- and flame-retardant performance of the vermiculite clays were compared to organo-modified montmorillonite (Cloisite 30B) and needle-shaped sepiolite (Pangel S9). Electron microscope investigations revealed different structures and dispersion levels of the clay nanoparticles in the polymer matrix. Tensile tests showed that the addition of clays led to considerable improvements in Young's modulus without compromising the elongation at break. Compared to the neat polymer, all clays reduced the peak heat release rate and the smoke production rate in cone calorimeter testing. Surprisingly, the needle-shaped sepiolite clay and the two vermiculites outperformed the montmorillonite organoclay in the fire testing even though it featured the highest degree of exfoliation in the polymer matrix.

**Keywords:** biopolymers; polyamides; clay; flame retardance

---

<sup>#</sup>Permanent address: Department of Chemical Engineering, Eduardo Mondlane University, PO Box 257, Maputo, Mozambique.

## **1. Introduction**

Polymers are used in many industrial applications. Their properties, including strength and stiffness, dimensional stability, flame retardancy, gas barrier properties, adhesive strength, UV stability or rheological properties, etc., can be enhanced by addition of clay-based nanoparticles [1-12]. A key requirement for optimum polymer property enhancement is extensive exfoliation into high aspect ratio, homogeneously dispersed sheets and this is conventionally achieved by suitable clay organo-modification in addition to appropriate mixing processes [8, 13-17].

Conventional polymer nanocomposites are prepared using surfactant modified clays. The nature of the surfactant plays an important role as it determines the degree of clay exfoliation that can be achieved. However, the surfactant molecules need to be chosen carefully such that interaction with the polymer chains in the matrix is favored above surfactant-clay and surfactant-surfactant interactions [5, 8]. Unfortunately cationic surfactants are prone to thermal degradation at the elevated temperatures employed in polymer processing. This motivated the search for a surfactant-free approach to the organo-modification of clays [18, 19] in addition to alternative ways to effect exfoliation, e.g. by sonication [19-25].

Polyamide 11 is a bio-based polymer derived from a renewable resource, i.e. castor oil [26, 27]. It can be flame retarded with phosphorus-based modifications [27]. However, the use of clay nanofillers is expected to simultaneously improve the mechanical performance. The present investigation considered vermiculite-based bionanocomposites prepared by surfactant-free organo-modification approaches as flame retardant for polyamide 11. Vermiculite exfoliates in a worm-like manner when heated to elevated temperatures. This form exfoliates easily using ultrasonic means. Good dispersion of such extensively delaminated vermiculite sheets are expected to significantly improve fire properties of polyamides. For comparison, the

fire performances of polyamide 11 in the presence of commercial organo-modified montmorillonite (Cloisite 30B) and sepiolite (Pangel S9) were also investigated. This allowed the effects of shape, aspect ratio, and degree of dispersion of the clay particles to be considered [28].

## **2. Experimental**

### **2.1 Materials**

Acetic acid 100% (glacial), ammonium chloride and deionized water were obtained from Merck Chemicals and used as received. An amorphous copolyamide, Euremelt 2138, was supplied by Huntsman Advanced Materials. According to the supplier, this copolyamide has a softening point in the range of 138 - 148 °C and an amine value of ca. 4 mg KOH g<sup>-1</sup> polymer. Polyamide 11 grades Rilsan BESNO TL and Rilsan BESNO P20 TL were supplied by Arkema, France. The latter grade contains 20 wt.% of an aromatic sulfonate ester plasticizer. According to the manufacturer, the melt volume index (MVI) measured per ISO 1133, for the two grades were 1 cm<sup>-3</sup> and 2 cm<sup>-3</sup> for BESNO TL and BESNO P20TL respectively. The MVI corresponds to the quantity of material at 235°C which flows in 10 minutes through a 2 mm diameter die under a 2.16 kg load.

Vermiculite grade Superfine (1 mm) from Palabora mining (South Africa) was obtained from Mandoval Vermiculite. Sepiolite grade Pangel S9 was supplied by Tolsa, Spain. According to the supplier, the BET surface area was 320 m<sup>2</sup>g<sup>-1</sup> and wet sieving left residues of 0.1%, 2% and 97.9% on sieves rated as 44 µm, 10 µm and 5 µm respectively. Cloisite 30B was manufactured by Southern Clay Products, USA. According to the supplier, the particle sizes were  $d_{10} = 2 \mu\text{m}$ ;  $d_{50} = 6 \mu\text{m}$  and  $d_{90} = 13 \mu\text{m}$  and the BET surface area is reported to be 7.74 m<sup>2</sup>g<sup>-1</sup>. The sepiolite Pangel S9 (PGS9) and Cloisite 30B (C30B) clays were used as received.

## ***2.2 Sample preparation***

The raw vermiculite was first washed with deionized water to remove soluble compounds and organic impurities by flotation. The washed material was then dried at 60 °C for 48 h. The ammonium exchanged vermiculite was prepared according to the following procedure [18]: 100 g of vermiculite was suspended in 500 mL of a 1 M solution of  $\text{NH}_4\text{Cl}$  ( $\text{pH} \approx 5$ ) and stirred for 2 h at ambient conditions and then left to stand overnight. The solid was separated by sedimentation and the supernatant decanted and replaced with fresh  $\text{NH}_4\text{Cl}$  solution. This procedure was repeated five times. Thereafter the  $\text{NH}_4^+$ -vermiculite was washed repeatedly with large volumes of deionized water until all chloride ions were removed (checked with  $\text{AgNO}_3$  solution). The recovered flakes were allowed to air dry.

Thermal exfoliation was achieved by exposing the material for 5 min to a temperature of 700 °C in a furnace [18]. Approximately 2 g of expanded material was suspended in 300 mL of deionized water. Ultrasonication was performed for 2 h at a power setting of 300 W using a Vibracell VC375 ultrasonic generator with a 12.5 mm solid tip horn. During this time the dispersion was agitated continuously with a magnetic stirrer. The slurry was allowed to settle for 2 h. Thereafter, the supernatant dispersion was decanted. Water was added to the residue and the sonication repeated for another 2 h. This process was repeated for a third time at which stage the remaining residue was discarded. The three flake dispersions obtained in this way were combined. The suspended vermiculite flakes were recovered by filtration. This process was repeated numerous times in order to get sufficient material for compounding trials. Finally all material treated in this way was combined. It was heated to 150 °C and kept there for 48 h to remove all residual water.

Portions of the product was organo-modified according to the following procedure: The copolyamide, Euremelt 2138, was separately dissolved in acetic acid (concentration 16.67 wt.% polyamide). The vermiculite powder was dispersed in acetic acid to yield a 13.7 wt.% slurry that was then placed in the 5 L stainless steel container of a heavy duty blender. The polyamide solution was added drop by drop while maintaining intense stirring. After completing the addition, mixing was continued for another 50 min. Then, while stirring continued, distilled water was added in order to precipitate the organo-modified clay. The remaining liquid was decanted and the precipitate washed repeatedly with distilled water over a period of 6 days to ensure complete removal of the acetic acid. The distilled water was replaced on a daily basis. The resulting material was finally dried at room temperature for 5 days. The neat and organo-modified vermiculites were designated as UVMT and OVMT, respectively. Portions of these powders were used to prepare polymer nanocomposites and the remaining materials kept for further analysis.

A typical preparation procedure for the final polyamide 11 bio-nanocomposites was as follows: The clays were melt compounded with polyamide 11 to form products that contained either no filler, i.e. neat polyamide 11 or 10% clay. The neat polyamide 11 was a mixture of Rilsan<sup>®</sup> Atofina BESNO TL and Rilsan<sup>®</sup> Atofina BESNO P20 TL in the proportion of 5:22 by mass. Since the plasticized grade containing 20 wt.% of a proprietary plasticizer, the final compounds contained 14.7 wt.% plasticizer. The use of a plasticized blend was necessary as the extruder used was unable to handle compounds based on the neat, plasticizer-free, polymer. The compounding process was carried out on a Nanjing Only Extrusion Machinery Co., Ltd (Model TE-30/600-11-40) co-rotating twin-screw laboratory extruder (diameter = 30 mm, L/D = 40:1) operating at a feed rate of 2 kg h<sup>-1</sup>. The barrel temperature profile ranged from 70 to

230 °C and the screw speed was set at 27 rpm. The extruded strand was passed through a cooling water bath, pelletized, and finally dried in a convection oven at 40 °C for 4 days.

The pellets were dried overnight at 85 °C before further processing. Polymer test sheets were made by hot pressing for 15 min at a temperature of 180 °C. Standard dumbbell-shaped tensile specimens with a thickness of 2 mm (DIN EN ISO 527-2-1BA) were injection molded using a BOY 22 A HV machine with a screw diameter of 18 mm. The processing was carried out with the barrel temperatures set at 250 °C with the mould temperature set to 50 °C. The maximum injection speed was set to 40 mm s<sup>-1</sup>, the maximum holding pressure was 85 bar held for a time period of 5.5 s and the cycle time was 31 s.

### ***2.3. Sample characterization***

Particle size distribution of the vermiculite samples was determined using a Malvern Mastersizer 3000 instrument. The refractive indices applied were 1.520 (for vermiculite) and 1.330 (for water). BET specific surface area was determined with nitrogen gas in a Micrometrics Tristar II BET instrument. Prior to measurements, samples were degassed under vacuum (10<sup>-3</sup> mbar) at 100 °C for 24 h.

X-ray diffraction was conducted on a PANalytical X'Pert Pro powder diffractometer with an X'Celerator detector and variable divergence and receiving slits with Fe-filtered Co K $\alpha$  radiation ( $\lambda = 0.17901$  nm) in the  $2\theta$  range 2 - 60° at a scan rate of 1.0° min<sup>-1</sup>.

A Zeiss Ultra 55 FESEM field emission scanning electron microscope (FESEM) was used to study the morphology of the clay samples and the fracture surface morphology of the composites at 1 kV. The composite injection molded specimens were frozen in liquid nitrogen,

cryo-fractured and vacuum dried. The clay samples and fractured surface of the composite samples were coated with carbon prior to analysis. FESEM was also used to observe the morphologies of the char residue obtained after combustion. The samples were coated five times with a conductive layer of carbon prior to imaging using an EMITECH K950X sputter coater. A transmission electron microscope (TEM) (JEM 1200EX, JEOL, Tokyo, Japan) (acceleration voltage 100 kV) was used to study the morphological structure of bionanocomposites. The samples were cryo-sectioned using a diamond knife.

Thermogravimetric analysis (TGA) was performed on a Perkin Elmer Pyris 4000 TGA instrument using the dynamic method. About 15 mg of the sample (vermiculite or polymer) were placed in open 150  $\mu$ L alumina pans. Temperature was scanned at a rate of 10  $^{\circ}$ C  $\text{min}^{-1}$  with air flowing at a rate of 50  $\text{mL min}^{-1}$  and mass loss recorded from 50 to 950  $^{\circ}$ C.

The injection-molded bionanocomposite dog-bones were placed in a closed plastic container and kept at 25  $^{\circ}$ C and 50% RH for seven days before mechanical testing. Saturated magnesium nitrate solution was used to meet the required relative humidity. Tensile testing of the specimens was performed on a Lloyds Instruments LRX Plus machine fitted with a 5 kN load cell (ASTM D638). Initial grip separation and crosshead speed were set at 45 mm and 20  $\text{mm min}^{-1}$ , respectively. Tensile strength, elongation at break and Young's modulus were measured and the averages values for seven test specimens are reported.

The cone-calorimeter tests were performed on a Dual Cone Calorimeter (Fire Testing Technology, U.K.) according to ISO 5660-1. Three specimens of each sample formulation were tested. The dimensions of the samples were 100  $\times$  100  $\times$  3.0 mm. Each specimen was wrapped in aluminum foil and exposed horizontally to a 35  $\text{kW m}^{-2}$  external heat flux. A hold-

down frame was used to restrain excessive swelling of the samples. The exhaust gas flow rate was set at  $24 \text{ L s}^{-1}$ . The time to ignition was manually captured from the computer's keyboard. Other fire performance parameter, e.g. heat release rate, peak values, etc. were evaluated using the Fire Testing Technology "ConeCalc" software.

### **3. Results and discussion**

#### ***3.1 Characterization of the clays***

Detailed characterization of the initial and intermediate stages of the vermiculite modifications was reported elsewhere [18]. Here the focus is on the characteristics of the final vermiculite used as nanoflakes and obtained by thermal exfoliation and ultrasonic delamination.

**Scanning electron microscopy (SEM).** SEM micrographs of the two vermiculites, the Pangel S9 and the C30B powders are shown in Figure 1. The vermiculites feature an exfoliated structure with similar morphologies. However, the surface of the OVMT particles appear to have a coating and seem more highly agglomerated. This is consistent with the expected organo-modification by the polyamide chains. As expected, the ultrasound treatment led to a significant decrease in particle size from literature [18, 20, 21]. The ultrasonic comminution led to irregularly shaped particles. However on the whole, two-dimensional flakes were obtained. Figure 1(c) shows a SEM micrograph revealing the fibrous, needle-like morphology of the sepiolite particles.

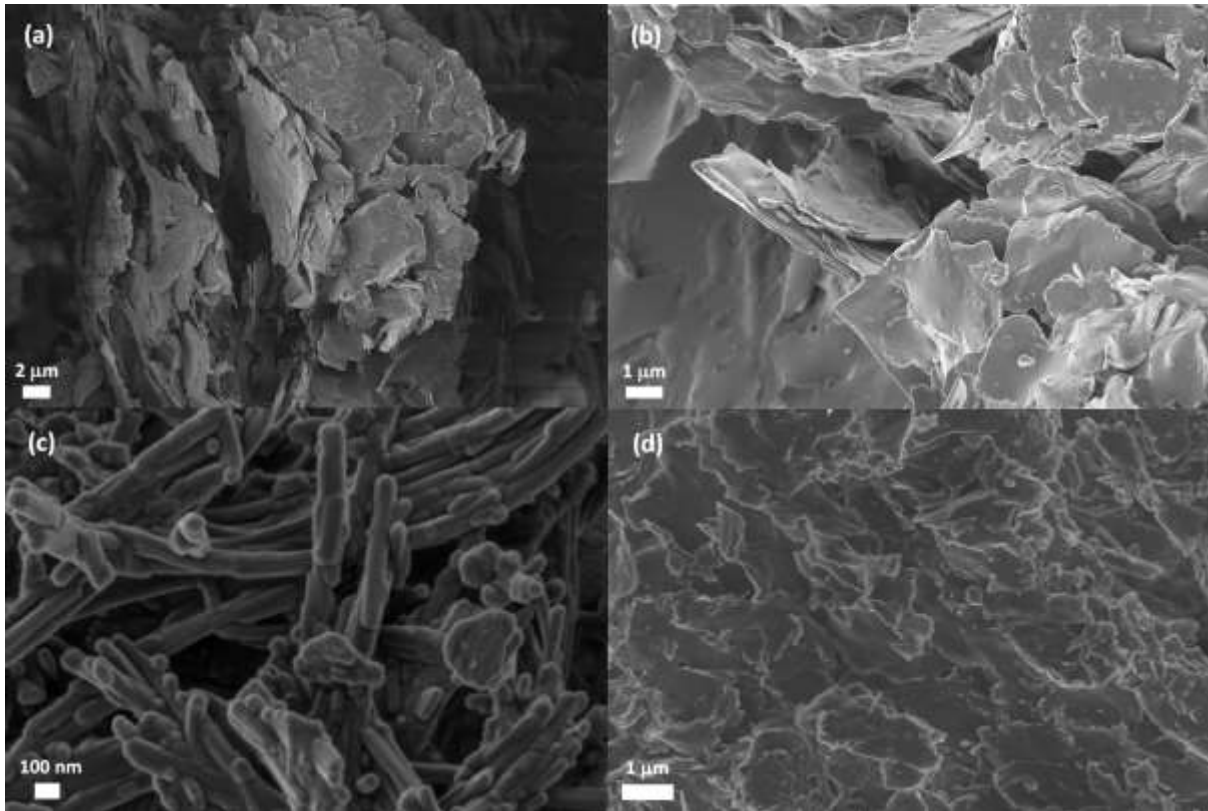


**Figure 1.** SEM micrographs of clay samples: (a) sonicated thermally exfoliated vermiculite (UVMT); (b) sonicated thermally exfoliated and organomodified vermiculite (OVMT); (c) sepiolite (PGS9); and (d) organo-modified montmorillonite (C30B).

**Particle size and BET surface area.** Particle size and BET surface area data for both the UVMT and OVMT samples are presented in Table 1. The values of particle size distribution and BET surface area of Pangel S9 were taken from the technical data sheets provided by the manufacturers. According to Table 1, the ammonium treatment of vermiculite did not result in a change in particle size. However, the  $d_{50}$  particle size value of the  $\text{NH}_4^+$ -exchanged vermiculite ( $879 \mu\text{m}$ ) was reduced to  $25.3 \mu\text{m}$  after sonication. By comparison, agglomeration of the organo-modified vermiculite resulted in an apparent increase in the particle size to  $139 \mu\text{m}$ . The sonication also caused an increase in the BET specific surface. Table 1 indicates that the BET specific surface area of the ammonium vermiculite was  $1.58 \text{ m}^2\text{g}^{-1}$ . After sonication

this increased to 11.4 and 8.78 m<sup>2</sup>g<sup>-1</sup> for UVMT and OVMT, respectively. These results are consistent with the SEM observations (see Figure 1).

**Table 1.** Particle size (μm) and BET surface area of the powder samples

Sample	$d_{10}$	$d_{50}$	$d_{90}$	BET (m <sup>2</sup> g <sup>-1</sup> )	$t^*$ (nm)
Neat - VMT	423	890	1760	1.49	525
NH <sub>4</sub> <sup>+</sup> -VMT	421	879	1750	1.58	496
UVMT	6.21	25.3	104	11.4	69
OVMT	46.8	139	481	8.78	89

\*Average flake thickness estimated from the BET specific surface area.

The average flake thickness was estimated from the BET specific surface area using the expression  $t = 2/(\rho A_{\text{BET}})$ , where  $t$  is the average flake thickness in m,  $\rho$  is the density in kg m<sup>-3</sup>; and  $A_{\text{BET}}$  is the BET specific surface area in m<sup>2</sup> kg<sup>-1</sup>. In this equation the edge surface area of the flakes was neglected. Assuming a density of  $\rho = 2.55 \text{ g cm}^{-3}$ , applying this equation indicates an average flake thicknesses of about 69 nm and 89 nm for UVMT and OVMT respectively, i.e. confirming the nano-size thickness for both vermiculites. This estimate does not take into account surface increasing defects, e.g. surface irregularities on the flakes.

**X-ray diffraction (XRD).** Figure 2(a) shows the XRD patterns of the sonicated UVMT and OVMT as well as PGS9 samples. Figure 2(b) shows the patterns for the corresponding bionanocomposites. PGS9 shows a strong diffraction peak at  $2\theta = 8.47^\circ$  equivalent to a basal spacing of 1.21 nm. The XRD data for the vermiculate samples were previously discussed [18, 29, 30]. The neat vermiculite (not shown here) features multiple reflections, suggesting a mixed layer structure of vermiculite phase (1.43 nm reflection) and mica (biotite/phlogopite) with a 1.00 nm reflection. The “hydrobiotite” features reflections at 2.441 nm and 1.221 nm

corresponding to the lattice planes (001) and (002) respectively [31, 32]. The main peak, with an extensive line broadening was found to be located at higher angles, suggesting a random distribution of the vermiculite and biotite layers. As reported in a previous work [18], a broadening of the “hydrobiotite” reflections was observed in the diffractograms of both UVMT and OVMT indicating delamination of vermiculite sheets due to sonication.

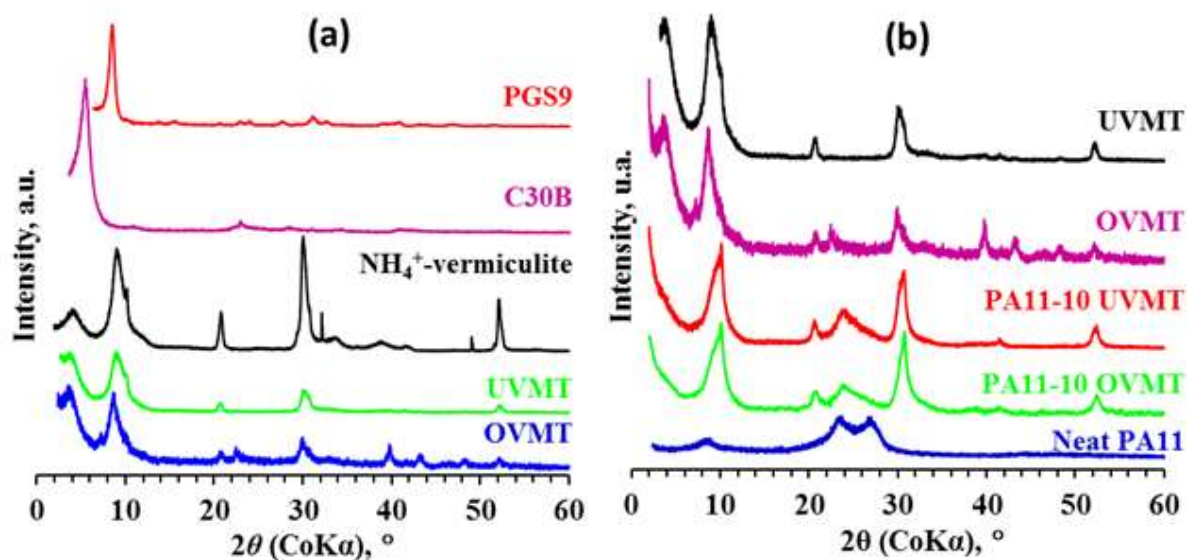


**Figure 2.** XRD patterns of (a) neat clays, and (b) the corresponding clay bionanocomposites

**Thermogravimetric analysis (TGA).** Figure 3 shows the TGA curves in air environment of UVMT, OVMT, PGS9, and C30B. Mass loss proceeds stepwise in all samples in the temperature range from 50 to 950 °C. This is related to the loss of physisorbed and interlayer water at lower temperatures and mass loss due to dehydration of hydroxyl groups at elevated temperatures. The UVMT sample only featured two main mass loss events. The decomposition onset temperatures for OVMT and C30B samples were above 200 °C. As expected, the OVMT and C30B clay samples showed a higher mass loss in the range 300 °C and 950 °C. The increased mass loss is attributed to the associated organic components, i.e. thermal decomposition of the surfactant (bis-(2-hydroxyethyl) methyl tallow alkylammonium) and the dimer fatty acid polyamide used as organomodifiers in C30B and OVMT, respectively.

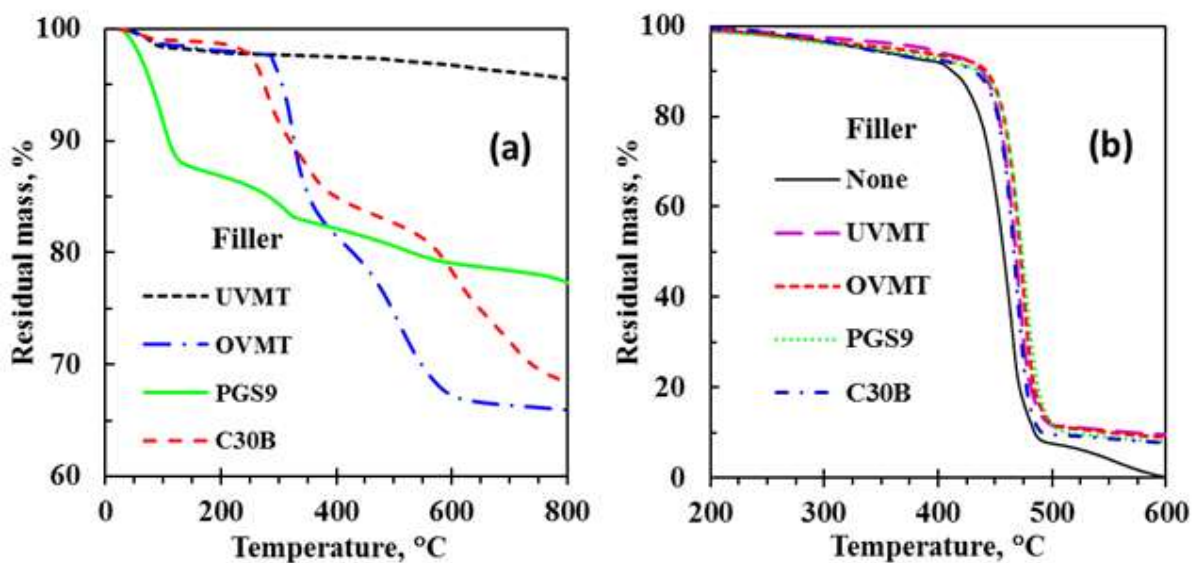


**Figure 3.** (a) TGA curves in air environment of the various clay samples. (b) TGA curves of neat polyamide 11 and its nanocomposites containing 10 wt.% modified clay.

The sepiolite sample also showed a higher mass loss despite the fact that the clay sample was dried at 60 °C for 24 h before testing. This suggests the presence of a higher amount of hygroscopic and zeolitic water. The main mass loss events of the sepiolite occur in four regions temperature ranges: 25 - 150 °C, 150 - 350 °C, 350 - 650 °C and 650 - 850 °C. Heating sepiolite from room temperature to about 150 °C selectively removes water physically absorbed on the external surface of the clay and zeolitic water trapped inside the structural channels. The weight loss observed in the second and third region is attributed to the dehydration of the first structural water (also called coordinated or bonded water) and of the second structural water. The final region corresponds to the dehydroxylation of internal Mg–OH resulting in a loss of the sepiolite structure. It is clear that UVMT is thermally the most stable clay considered presently.

### **3.2. Morphology and properties of the PA11-clay bionanocomposites**

**X-ray diffraction analysis (XRD).** X-ray diffraction patterns for C30B, PGS9, UVMT and OVMT in neat and in bionanocomposite form are shown in Figure 2(b). Polyamide 11 exhibits

three main crystalline reflection peaks at about  $2\theta = 8.3, 23.4$  and  $26.6^\circ$  corresponding to (001), (100) and (010/110) planes, respectively. These crystalline peaks correspond to those of the  $\alpha$ -polymorph of Polyamide 11, typically developing on slow melt-crystallization [33, 34].

Compared to the XRD patterns for neat PGS9, no change in clay reflections were observed for the corresponding bionanocomposite (not shown in Figure 2(b)). The reflection at  $2\theta = 8.47^\circ$  in the bionanocomposite is due to the sepiolite structure. Exfoliation of smectite clays refers to the complete separation of clay sheets followed by dispersion of throughout the polymer matrix. This is not possible for the fibrous sepiolite with a structure where individual tetrahedral-octahedral-tetrahedral layers are strongly held together by covalent bonds. The fiber bundles or aggregates can separate into nanometer-dimension structures which may then be dispersed throughout the polymer matrix. Therefore, even the complete fibrillation of the sepiolite needles (non-swelling clay) will hardly have an effect on the location of the diffraction peak in the XRD pattern. This explains why no shift of the position clay reflection was observed in the XRD pattern for the bionanocomposite [35-39].

For the UVMT- and OVMT-based bionanocomposites, the XRD patterns shown in Figure 2(b) correspond to those of the neat clays. This implies that the compounding step did not lead to any additional exfoliation to individual vermiculite sheets. Rather, the nanoflakes were probably retained as they were. The  $2\theta = 5.46^\circ$  reflection for the C30B is also observed in the XRD diffractogram of the corresponding nanocomposite. This means that the compounding process failed to produce complete exfoliation of the smectite clay.

**Electron microscopy (SEM and TEM).** The fracture surface morphology of the bionanocomposites was studied by FESEM. Representative images of the morphology and

orientation of different clays in the polyamide 11 bionanocomposites are shown in Figure 4. Vermiculite sheets appear well-dispersed but somewhat aligned as illustrated in Figures 4(a) and (b). Furthermore, vermiculite particles in the polyamide matrix appear mostly as relatively large sheets (in the micrometer range) with a distribution of thicknesses that extends into the nanometer range. The presence of thicker sheets was expected since the vermiculite used as raw material consisted of flakes that correspond to randomly interstratified vermiculite-biotite layers [30]. The material basically derived from incomplete weathering of the biotite part. So, the thicker sheets are probably thick biotite layers. The presence of mica impurities with higher charge densities also makes it difficult to exfoliate this vermiculite under the processing conditions that were employed. Cleavage of the vermiculite, which probably happened during the cryogenic fracturing, is clearly visible in 4(a) and 4(b). Interestingly, Figure 4(b) shows roopy polymer structures connecting two vermiculite flakes.

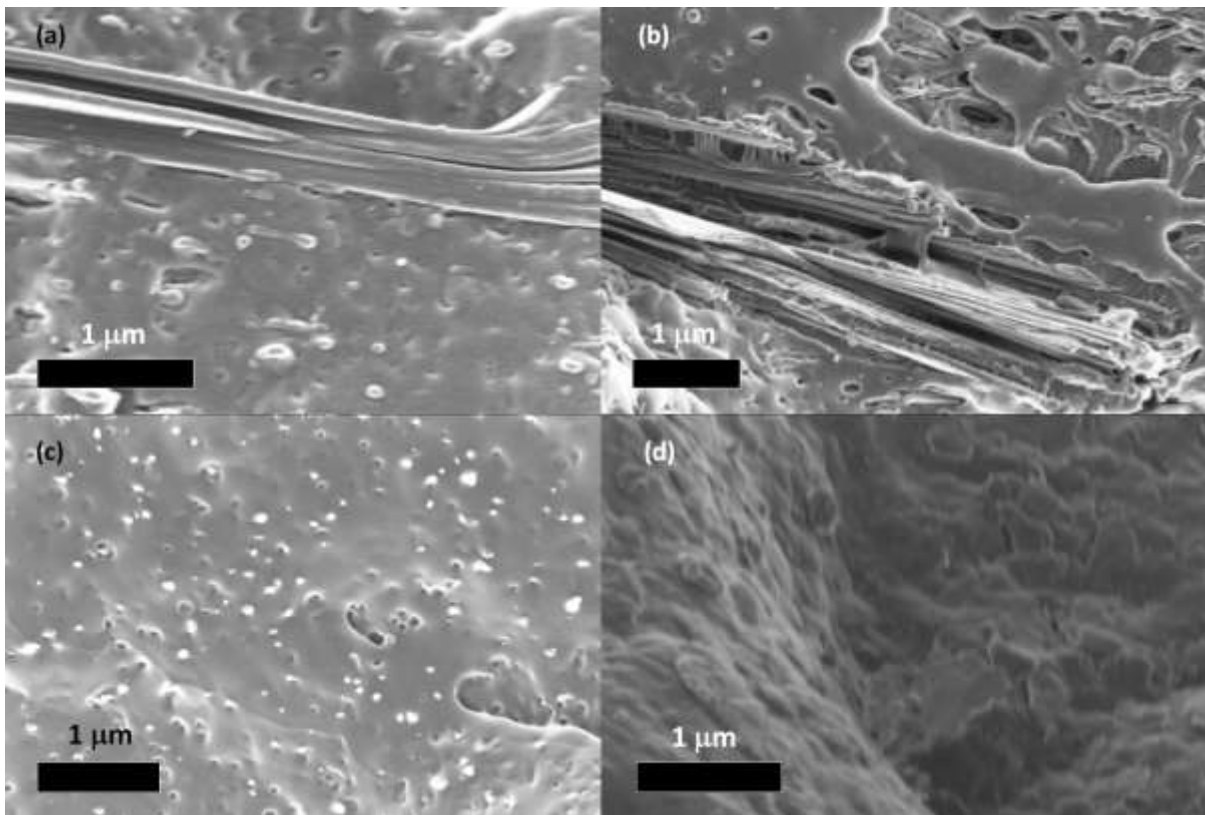


**Figure 4.** Cross sectional SEM images of polyamide 11 nanocomposites containing 10 wt.% of (a) UVMT, (b) OVMT, (c) PGS9, and (d) C30B.

Preferred orientation was also observed in the bionanocomposites filled with PGS9 and C30B as indicated in Figure 4(c) and 4(d). The images show excellent dispersion of the fibrous sepiolite and the montmorillonite layers in the polyamide matrix. Individual broken sepiolite needles protrude from the surface and small bundles (in white color) are visible on the fracture surface in Figure 4(c). The fact that the fibers fractured indicates that they were well wetted and strongly bonded into the polymer matrix. The situation is not very clear for the C30B composite but clay flakes are visible on the fracture surface.

Better evidence regarding the local dispersion of the clays in polyamide matrix was obtained from the TEM images. Figure 5 shows representative TEM micrographs of microtome cut cross-sections taken from polyamide 11 clay bionanocomposites. The dark lines represent the thickness of individual clay layers, sepiolite needles or their agglomerates, whereas the gray or white areas represent the polyamide matrix. In general, all micrographs reveal uniformly dispersion of all clays in the polyamide 11 matrix and also excellent exfoliation for the C30B. The mean thickness of the clay sheets varied from tens of nanometers (vermiculites) to just a few nanometers (C30B). A good nano-dispersion was also obtained with sepiolite in polyamide 11 as shown in Figure 5(c). This can be attributed to strong interactions between the polymer and sepiolite through hydrogen bonding between the carbonyl groups of the polymer and the hydroxyl groups situated at the edges of sepiolite. The presence of hydroxyl groups in the sepiolite structure makes organic modification unnecessary [36].

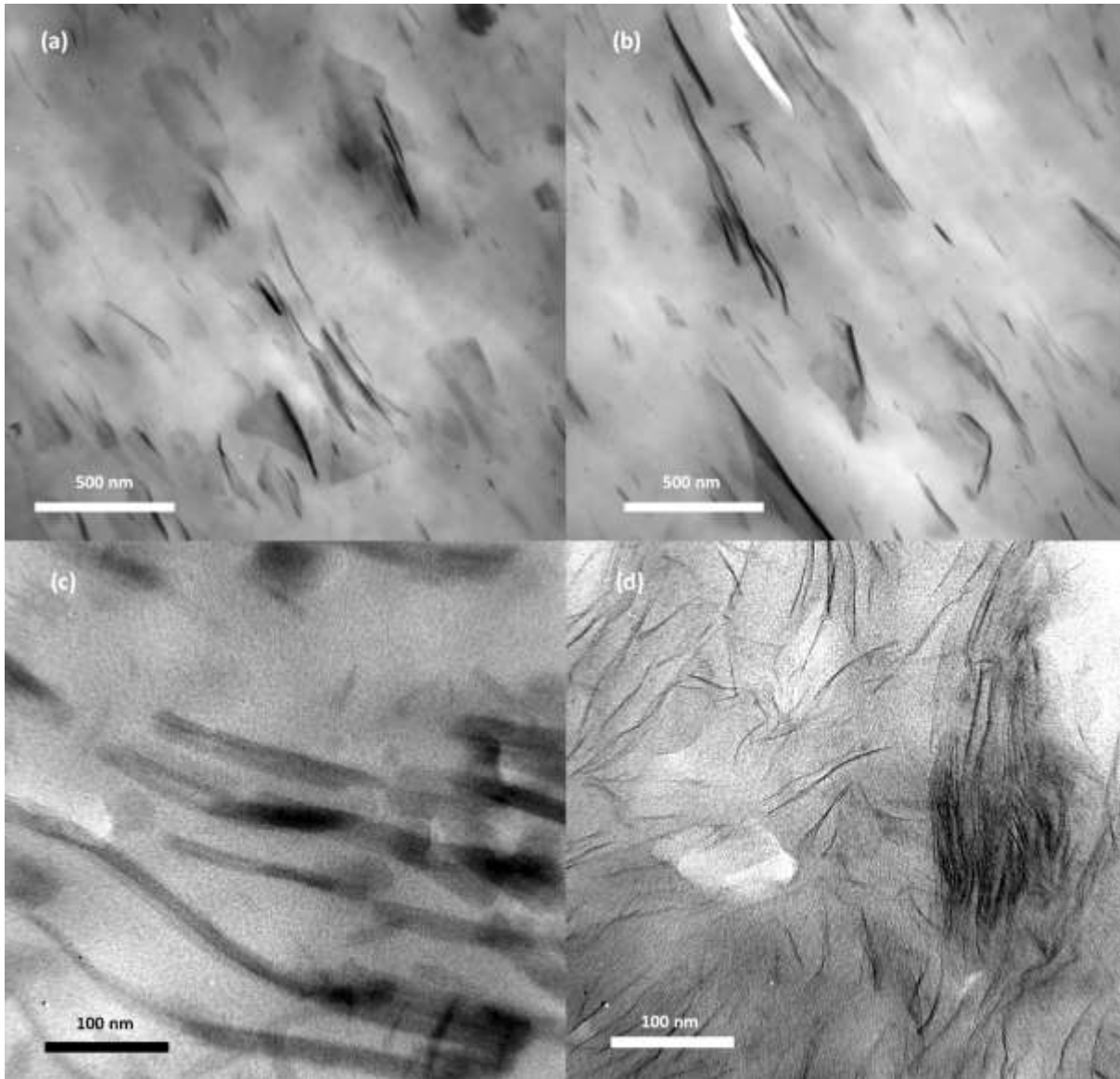


**Figure 5.** TEM images of polyamide 11 bionanocomposites containing 10 wt.% of (a) UVMT, (b) OVMT, (c) PGS9, and (d) C30B.

**Thermogravimetric analysis (TGA).** Figure 3(b) presents the variation of mass loss with temperature recorded in an air atmosphere for the neat polyamide blend and the various clay bionanocomposites. The TGA curves for the neat polyamide shows gradual mass loss between 200 °C and 410 °C. At this point the mass remaining is about 92%. Then much more rapid mass loss occurs and by 490 °C the residue only amounts to about 10%. Above this temperature the remaining char slowly loses mass and at a temperature of ca. 600 °C nothing remains. The

two-step mass loss process in the plasticized polyamide blend could be due to a catalytic charring effect caused by the presence of the aromatic sulfonate ester plasticizer. Alternatively, it might result from the charring of the plasticizer itself. Further investigation will be necessary to fully determine the true mechanism is but this is beyond the scope of the present study.

The mass loss curves for the bionanocomposites has a similar shape except that the curves are shifted to higher temperatures and that at the end the mass loss approaches a plateau value commensurate with the relevant inorganic clay residue. The thermal stability of the bionanocomposites appears to be higher by about 10 °C than that of the neat polyamide under the specific chosen thermo-oxidative degradation conditions. This is expected since the apparent thermal stability derives from mass transport barrier effects caused by the presence of the impermeable clay sheets. This reduces the rate of oxygen diffusion into the matrix and the release, to the atmosphere, of small molecule fragments generated during thermal decomposition [39]. Figure 3(b) shows that, compared to neat polymer, the degradation onset temperature is slightly higher for the bionanocomposites.

**Tensile properties.** Tensile properties of the neat polyamide 11 and its bionanocomposites are listed in Table 2. Both tensile strength and Young's modulus are improved by incorporating the clay fillers. However, the improvement is more pronounced for the Young's modulus with the value about double that for the neat polymer. This is achieved without loss of the elongation at break except for the PGS9 where it is reduced from 190% to 90%. The improvement in tensile strength and modulus is due to the stiffness of the clays. The facts that an increase in tensile strength was observed and the elongation at break did not decrease suggests that there was adequate adhesion between the matrix polymer and the filler particles. Interestingly, the addition of vermiculite (OVMT and UVMT) or C30B actually led to an increase in elongation

at break. Similar results were previously reported for EVA nanocomposites [40]. This type of behavior has been explained by considering conformational effects at the clay-matrix interface [41].

**Table 2.** Tensile properties of polyamide 11-clay bionanocomposites

Sample	Tensile strength (MPa)	Young's modulus (MPa)	Elongation at break (%)
PA-11	46.9±1.4	276±10	190±12
OVMT	49.6±1.7	527±19	200±12
UVMT	57.8±2.1	550±25	222±15
PGS9	60.5±0.4	610±13	90±14
C30B	60.5±2.7	509±12	227±14

**Flame retardancy of polyamide 11/clay bionanocomposites.** The cone calorimeter results are presented in Figure 6 and summarized in Table 3. Figure 6(a) shows representative heat release rate (*HRR*) curves obtained from the cone calorimeter tests. The neat polyamide 11 sample ignited and burned rapidly giving rise to a sharp peak in the *HRR*. This shape is characteristic of thermally thin samples [42]. *HRR* curves characteristic of thermally thick, char-producing samples show a sudden rise to a plateau value [42]. This was the case for all the bionanocomposite samples as seen in Figure 6(a). Compared to the neat polyamide 11 compound, the maximum value of the *HRR* was much reduced in intensity. According to the results tabulated in Table 3, the *pHRR* for the neat polyamide compound was  $575 \pm 53 \text{ kW m}^{-2}$ . The best *pHRR* result was obtained with OVMT ( $299 \pm 2 \text{ kW m}^{-2}$ ) while the C30B-based nanocomposite performed worst at  $353 \pm 39 \text{ kW m}^{-2}$ . Adding the clays appears to have increased the total heat release (*tHR*) from  $89 \pm 15 \text{ MJ m}^{-2}$  to values close to  $100 \text{ MJ m}^{-2}$ . However, the difference is not statistically significant considering the large standard

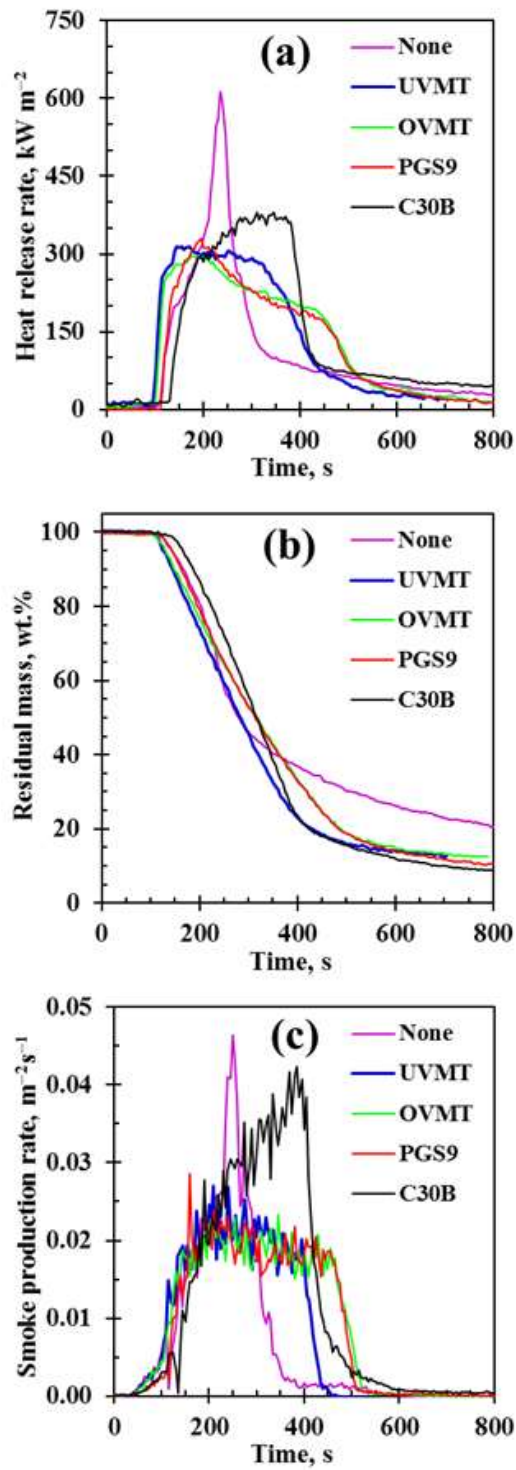


**Figure 6.** (a) Heat release rate (HRR); (b) residual mass, and (c) smoke production rate for neat polyamide 11 and its nanocomposites during the cone calorimeter test conducted at a flux of  $35 \text{ kW m}^{-2}$ .

**Table 3.** Cone calorimeter fire test data for polyamide 11 bionanocomposites

Property	Units	Clay filler				
		None	UVMT	OVMT	PGS9	C30B
Time to ignition	s	110 ± 5	101 ± 1	104 ± 1	117 ± 3	138 ± 6
Time to flameout	s	> 800	633 ± 45	685 ± 59	721 ± 52	933 ± 42
Peak heat release rate	kW m <sup>-2</sup>	575 ± 53	321 ± 9	299 ± 2	318 ± 16	353 ± 39
Total heat release	MJ m <sup>-2</sup>	89 ± 15	99 ± 6	98 ± 2	93 ± 2	112 ± 8
<i>FIGRA</i>	kW m <sup>-2</sup> s <sup>-1</sup>	333 ± 10	64 ± 2	60 ± 1	64 ± 3	70 ± 8
<i>MARHE</i>	kW m <sup>-2</sup>	177 ± 1	213 ± 1	194 ± 1	179 ± 1	201 ± 1

deviation for the value measured for the neat polymer. The *tHR* was the highest for C30B at  $112 \pm 8 \text{ MJ m}^{-2}$ . Figure 6(b) shows representative mass loss vs. time recorded during the cone tests. Beyond 300 s the Cone calorimeter mass loss curve for the neat polyamide 11 tapers off indicating that a thermally stable char had formed. However, this was not the case for the bionanocomposites mass loss curves. All of them only approached plateau values at much higher temperatures and at residue level approached values just above the expected ash content. This means that all the clays must have catalyzed the combustion of residual polyamide-derived char. This explains the higher *tHR* values for the bionanocomposites.

The time to ignition ( $t_{ig}$ ) was  $110 \pm 5$  s for the neat polyamide 11 compound. The C30B performed better with respect to this fire parameter as the time of ignition increased to  $138 \pm 6$  s. The UVMT performed worst with  $t_{ig} = 101 \pm 1$  s. The decrease in ignition times might be attributed to changes in thermos-radiative properties leading to a faster heating of the polymer surface [43].

Figure 6(c) compares the smoke production rates (*SPR*) of the bionanocomposites with that for the neat polyamide 11 compound. The composites based on the vermiculites featured lower *SPRs* but smoke emission lasted longer. The C30B-based compound performed poorly, producing high levels of smoke for a much longer time.

The fire growth rate (*FIGRA*) and the maximum average rate of heat emission (*MAHRE*) are fire performance indices that are used to interpret cone calorimeter data [42, 44]. The *FIGRA* is an estimator for the fire spread rate and size of the fire whereas the *MAHRE* guesstimates the tendency of a fire to develop [44]. The *FIGRA* is defined as the maximum quotient of  $HRR(t)/t$ . Table 3 lists the *FIGRA* and *MAHRE* indices. There was a marked decrease in the *FIGRA* for all clays but a small increase in the *MAHRE* was observed.

**Morphologies of char residues and flame retardancy mechanism.** Figure 7 shows photographs of the residues at the end of the cone calorimeter tests. Combustion clearly led to considerable expansion for the vermiculite- and sepiolite-based samples. The ash residue formed a cohesive structure with a smooth surface. The C30B sample also resulted in a cohesive residue but there was little expansion and the surface featured a coarse granular appearance. Figure 8 shows SEM images of the inner microstructure of the ash residues. It shows that in all cases the clay particles formed foamed structures built up by large scale particle agglomeration. The reduction of the heat release rate is attributed to the barrier properties provided by the cohesive residues.

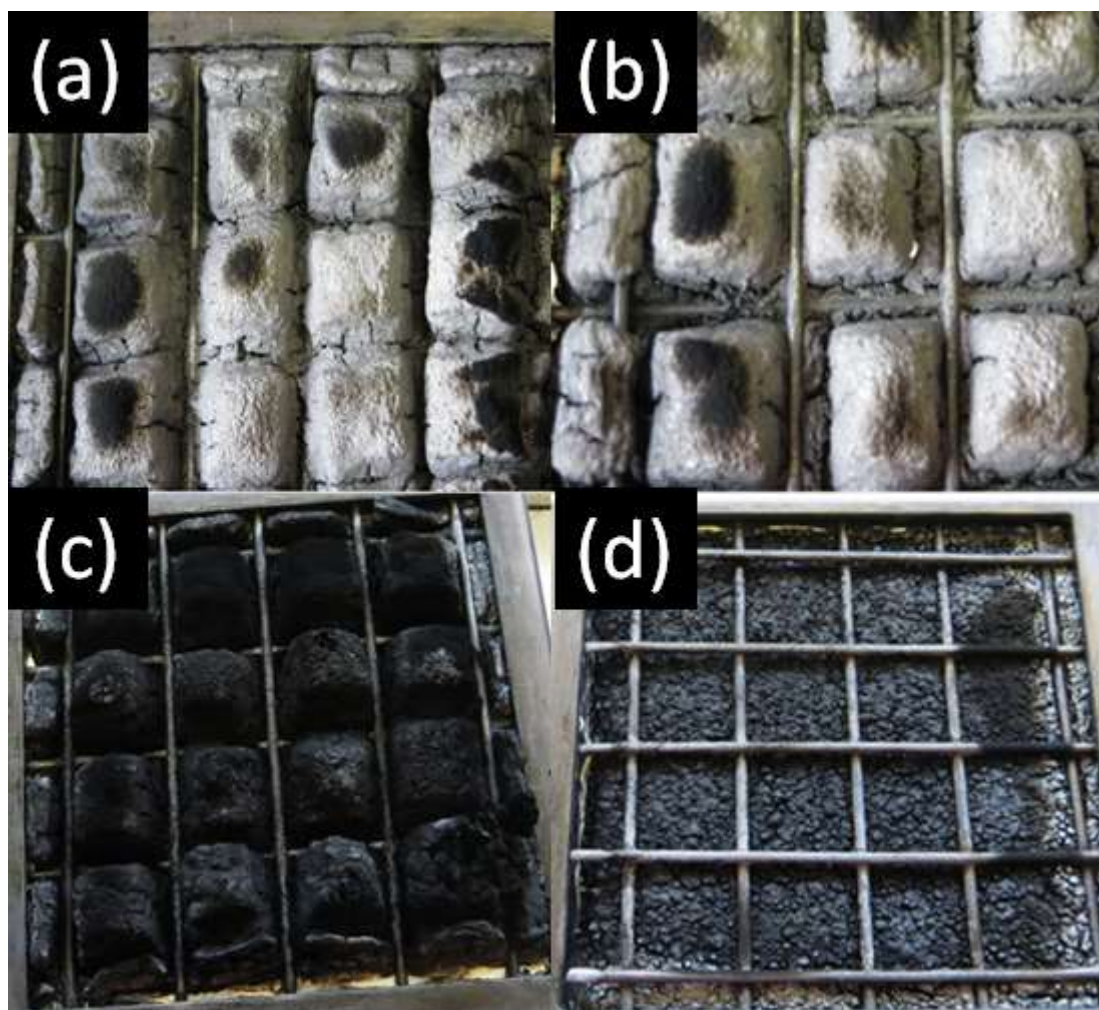


**Figure 7.** Digital photographs of the char residues of polyamide 11 flame retardant nanocomposites after cone calorimeter test: (a) UVMT, (b) OVMT, (c) PGS9, and (d) C30B.

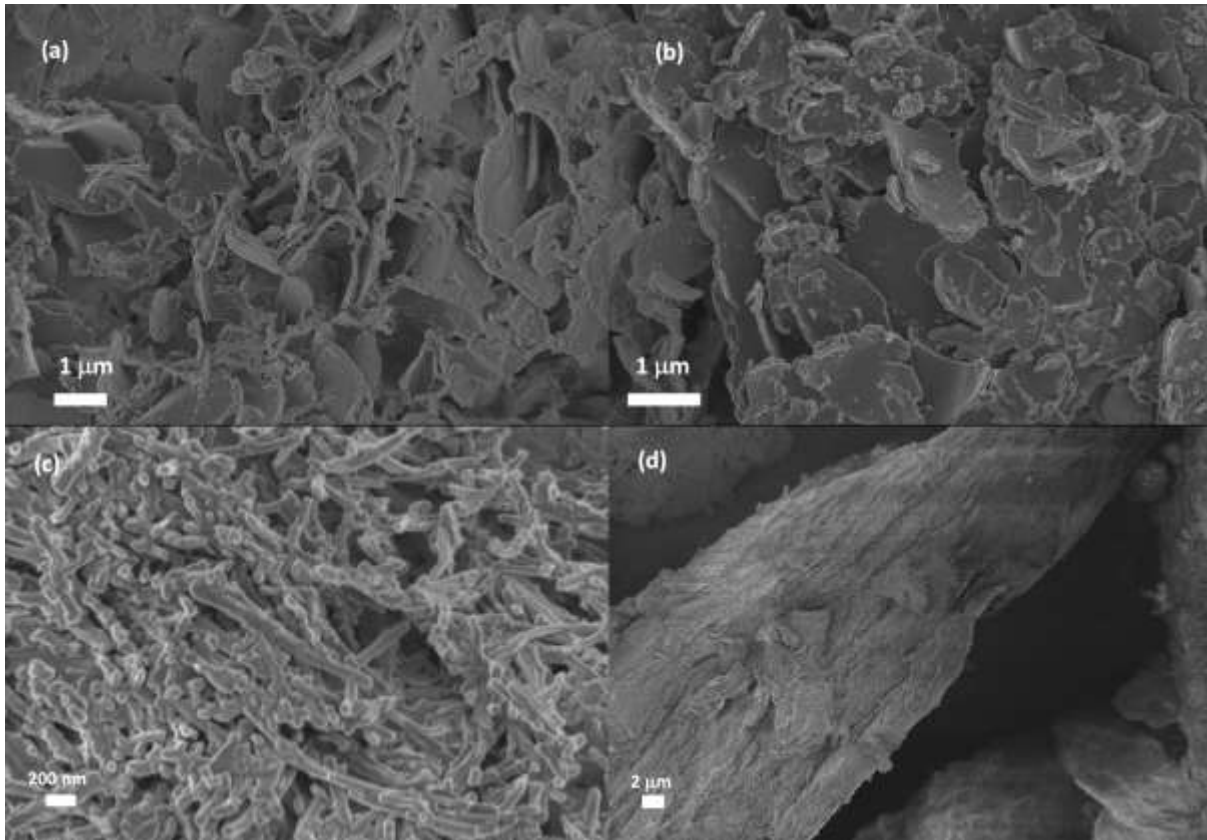


**Figure 8.** SEM images of the char residues of polyamide 11 bionanocomposites obtained from cone-calorimeter test: (a) UVMT, (b) OVMT, (c) PGS9, and (d) C30B

#### 4. Conclusions

Vermiculite was successfully pre-exfoliated into nanoflakes by ultrasonic treatment of thermal shock-expanded material. Organic surface modification with amine terminated dimer acid-polyamide was achieved by ion exchange in acetic acid. Polyamide 11-based bionanocomposites were successfully prepared by melt compounding using both vermiculite types. The clay content was set at 10 wt.%. Two additional nanocomposites were prepared for comparison purposes. They were needle-shaped sepiolite (Pangel S9) and a flake-shaped organo-modified smectite clay (Cloisite 30B). Transmission electron microscopy revealed the presence of vermiculite flakes with a thickness less than 100 nm but with lateral dimensions extending into the micron range. This means that vermiculite particle morphology was not changed by the compounding process. However, the C30B nanocomposite contained essentially clay sheets, small tactoids and clay flakes while for the sepiolite dispersed fibers

and fiber bundles were observed. Scanning electron microscopy showed that, at larger scales, there was a uniform distribution of all these mixed morphology clay reinforcement inside nanocomposite matrix.

The presence of the clays increased the tensile strength marginally but the Young's modulus was almost double that of the neat polyamide 11 value. Except for the Cloisite 30B filler, this was achieved without compromising the elongation at break.

The fire behavior of the neat polymer and the bionanocomposites was studied by cone calorimetry. Compared to the neat polyamide 11, the addition of the clays resulted in a larger total fire load and slightly increased the risk for a fire to develop. This is attributed to the clay catalyzing the oxidation of the polyamide-derived char. However, incorporating the clays is expected to dramatically reduce the rate of fire spread and also to reduce the smoke production rate. In the latter aspect Cloisite 30B was the exception in that the smoke production remained high for longer.

The main conclusion is that pre-exfoliated vermiculite, whether in neat or organo-modified form, can provide similar or better mechanical property enhancement in addition to improved fire behavior than the fibrous sepiolite and a conventional organo-modified smectite clay.

### **Acknowledgements**

Financial support for this research from the Deutsche Forschungsgemeinschaft (DFG) through Grant AN 212/18-1 and from the National Research Foundation (NRF) via the South African/Algeria research partnership program under Grant 87453 is gratefully acknowledged.

Any opinion, finding and conclusion or recommendation expressed in this material is that of the authors and the DFG and the NRF do not accept any liability in this regard.

## References

1. P. Kiliaris, and C. Papaspyrides, *Prog. Polym. Sci.* **35**, 902 (2010).
2. S.J. Ahmadi, Y. Huang, and W. Li, *Compos. Sci. Technol.* **65**, 1069 (2005).
3. M. Alexandre, and P. Dubois, *Mater. Sci. Eng., R* **28**, 1 (2000).
4. A. Arora, and G. Padua, *J. Food Sci.* **75**, R43 (2010).
5. L.B. de Paiva, A.R. Morales, and F.R.V. Díaz, *Appl. Clay Sci.* **42**, 8 (2008).
6. L.A. de Sousa Rodrigues, A. Figueiras, F. Veiga, R.M. de Freitas, L.C.C. Nunes, E.C. da Silva Filho, and C.M. da Silva Leite, *Colloids Surf. B* **103**, 642 (2013).
7. H. Fischer, *Mater. Sci. Eng. C* **23**, 763 (2003).
8. P.C. LeBaron, Z. Wang, and T.J. Pinnavaia, *Appl. Clay Sci.* **15**, 11 (1999).
9. J. Lee, and H. Lee, *Mater. Chem. Phys.* **85**, 410 (2004).
10. S.S. Ray, and M. Okamoto, *Prog. Polym. Sci.* **28**, 1539 (2003).
11. L.A. Utracki, *Nanosci. Nanotechnol.* **8**, 1582 (2008).
12. S. Wang, Y. Hu, R. Zong, Y. Tang, Z. Chen, and W. Fan, *Appl. Clay Sci.* **25**, 49 (2004).
13. T. Gopakumar, J. Lee, M. Kontopoulou, and J. Parent, *Polymer* **43**, 5483 (2002).
14. S. Pavlidou, and C. Papaspyrides, *Prog. Polym. Sci.* **33**, 1119 (2008).
15. C.E. Powell, and G.W. Beall, in J.E. Mark (Ed.) *Physical properties of Polymers Handbook*, Springer: New York (2007).
16. Y. Yang, Z.-K. Zhu, J. Yin, X.-y. Wang, and Z.-E. Qi, *Polymer* **40**, 4407 (1999).
17. D.J. Chaiko, and A.A. Leyva, *Chem. Mater.* **17**, 13 (2005).
18. A. Macheca, D. Gnanasekaran, and W.W. Focke, *Colloid Polym. Sci.* **292**, 669 (2014).
19. A.D. Macheca, W.W. Focke, H.F. Muiambo, and M. Kaci, *Eur. Polym. J.* **74**, 51 (2016).
20. F. Ali, L. Reinert, J.-M. Lévêque, L. Duclaux, F. Muller, S. Saeed, and S.S. Shah, *Ultrason. Sonochem.* **21**, 1002 (2014).
21. M. Kehal, L. Reinert, and L. Duclaux, *Appl. Clay Sci.* **48**, 561 (2010).
22. L. Pérez-Maqueda, O. Caneo, J. Poyato, and J. Pérez-Rodríguez, *Phys. Chem. Miner.* **28**, 61 (2001).
23. J. Pérez-Rodríguez, F. Carrera, J. Poyato, and L. Pérez-Maqueda, *Nanotechnology* **13**, 382 (2002).
24. J. Poyato, J. L. Pérez-Rodríguez, V. Ramírez-Valle, A. Lerf, and F. E. Wagner, *Ultrason. Sonochem.* **16**, 570 (2009).
25. A. Wiewiora, J. Pérez-Rodríguez, L. Pérez-Maqueda, and J. Drapała, *Appl. Clay Sci.* **24**, 51 (2003).
26. P.J. Halley, and J.R. Dorgan, *MRS Bull.* **36**, 687 (2011).
27. C. Negrell, O. Frénéhard, R. Sonnier, L. Dumazert, T. Briffaud, and J.J. Flat, *Polym. Degrad. Stab.* **134**, 10 (2016).
28. L.A. Utracki, B. Broughton, N. González-Rojano, L.H. de Carvalho, and C.A. Achete, *Polym. Eng. Sci.* **51**, 559 (2011).
29. O. Folorunso, C. Dodds, G. Dimitrakakis, and S. Kingman, *Int. J. Miner. Process.* **114**, 69 (2012).
30. H.F. Muiambo, W.W. Focke, M. Atanasova, I. Van der Westhuizen, and L.R. Tiedt, *Appl. Clay Sci.* **50**, 51 (2010).

31. A.R. Amil, F.A. de la Cruz, E. Vila, and A.R. Conde, *Clay Miner.* **27**, 257 (1992).
32. A. Newman, and G. Brown, The Chemical Constitution of Clays, in A. Newman (Ed.) *Chemistry of Clays and Clay Minerals*. Mineralogical Society Monograph No. 6, John Wiley and Sons:New York (1987)
33. A. Mollova, R. Androsch, D. Mileva, C. Schick, and A. Benhamida, *Macromolecules* **46**, 828 (2013).
34. A.M. Rhoades, N. Wonderling, C. Schick, and R. Androsch, *Polymer* **106**, 29 (2016).
35. A. Choudhury, A.K. Bhowmick, and C. Ong, *J. Appl. Polym. Sci.* **116**, 1428 (2010).
36. K. Fukushima, D. Tabuani, and G. Camino, *Mater. Sci. Eng. C* **32**, 1790 (2012).
37. K.D. Kumar, A.H. Tsou, and A.K. Bhowmick, *Macromolecules* **43**, 4184 (2010).
38. Z.-C. Qiu, J.-J. Zhang, Y. Niu, C.-L. Huang, K.-K. Yang, and Y.-Z. Wang, *Ind. Eng. Chem. Res.* **50**, 10006 (2011).
39. Z. Liu, K. Chen, and D. Yan, *Polym. Test.* **23**, 323 (2004).
40. L. Moyo, W.W. Focke, D. Heidenreich, F.J.W.J. Labuschagne, and H.J. Radusch, *Mater. Res. Bull.* **48**, 1218 (2013).
41. P.H.C. Camargo, K.G. Satyanarayana, and F. Wypych, *Mater. Res.* **12**, 1 (2009).
42. B. Schartel, and T.R. Hull, *Fire Mater.* **31**, 327 (2007).
43. L. Ferry, R. Sonnier, J.M. Lopez-Cuesta, S. Petigny, and C. Bert, *J. Therm. Anal. Calorim.*, 1 (2017).
44. M. Sacristán, T.R. Hull, A. A. Stec, J.C. Ronda, M. Galià, and V. Cádiz, *Polym. Degrad. Stab.* **95**, 1269 (2010).

**.Published as:** Macheca, A. D., Focke, W. W., Kaci, M., Panampilly, B. and Androsch, R. (2018), Flame retarding polyamide 11 with exfoliated vermiculite nanoflakes. *Polym Eng Sci*, 58: 1746-1755. doi:10.1002/pen.24775

